Microscopy and Microanalysis (2019), **25**, 47–57
doi:10.1017/S1431927618015672

Microscopy AND Microanalysis

Original Article

Improved Accuracy for Trace Element Analysis of Al and Ti in Quartz by Electron Probe Microanalysis

Ji-Qiang Cui[1], Shui-Yuan Yang[1]*, Shao-Yong Jiang[1,2] and Jing Xie[3]

[1]State Key Laboratory of Geological Processes and Mineral Resources, China University of Geosciences, Wuhan 430074, PR China; [2]Faculty of Earth Resources and Collaborative Innovation Center for Scarce and Strategic Mineral Resources, China University of Geosciences, Wuhan 430074, PR China and [3]Key Laboratory of Continental Collision and Plateau Uplift, Institute of Tibetan Plateau Research, Chinese Academy of Sciences, Beijing 100101, PR China

Abstract

The trace elements in quartz, Al and Ti, contain considerable information about mineral genesis, and determining their concentrations is of great importance in geology. Electron probe microanalysis has the advantages of non-destructive testing and high spatial resolution; however, it is a challenge to improve the accuracy and precision of trace element detection using this method. The important factors affecting accuracy include the fragility of quartz lattices at high beam currents and the methods used to determine the background. In this paper, the peaks of Al-Kα and Ti-Kα, and their backgrounds, were found to exhibit intensity variations at high beam currents and small beam diameters; therefore, it is necessary to select a large beam diameter (up to 20 μm) to avoid variations in intensity at high currents (500 nA). For background determination of Al, a multipoint background method is proposed to determine the background value, which greatly improves the accuracy of the results. For Ti, the choice of background measurement does not affect the result. In addition, it is verified that the background obtained from other quartz samples can be used as the background of an unknown quartz sample, which reduces the analysis time and minimizes sample damage.

Key words: background determination, electron probe microanalysis, quartz, time-dependent intensity, trace elements

(Received 29 April 2018; revised 7 November 2018; accepted 27 November 2018)

Introduction

Quartz is a common mineral in the Earth's crust, formed in many geological environments. The concentration of trace elements in quartz provides considerable information about how the mineral was formed. For example, the temperature at the time of formation can be calculated by determining the Ti content of quartz (e.g., Larsen et al., 2004; Wark & Watson, 2006; Wiebe et al., 2007). The Al content in quartz is closely related to the content of Al in hydrothermal fluids, and the latter is influenced mainly by pH. Thus, the change in Al content in quartz can reflect changes in the fluid pH (e.g., Rusk et al., 2008). Quartz crystals formed at different stages (magmatic, hydrothermal, etc.) may have different cathodoluminescence (CL) textures and trace element compositions, as quartz possesses the geochemical signature of the medium where it crystallizes. By combining CL images with the distribution of trace elements such as Al, Ti, Ge, and K in quartz, the relationship between trace elements and CL textures can be established. As a result, quartz has been used to interpret geologic processes, including those in crustal metamorphism and anatexis, magma genesis and evolution, and hydrothermal ore formation (e.g., Müller et al., 2003a, 2010, 2015; Larsen et al., 2009; Breiter et al., 2012; Audétat, 2013; Tanner et al., 2013; Frelinger et al., 2015; Drivenes et al., 2016; Garate-Olave et al., 2017). Therefore, it is of crucial geological significance to accurately determine the concentration and distribution of trace elements in quartz. *In situ* microanalysis of trace elements by techniques such as laser ablation inductively coupled plasma mass spectrometry (LA-ICP-MS) has been widely used to obtain reliable results. However, LA-ICP-MS damages samples during analysis, and the large beam diameter (usually ranging from dozens to even a hundred micrometers) is required for trace element detection levels in quartz; thus, the spatial resolution is low. When the beam diameter of laser ablation is larger than the width of a thin mineral zone, a mixed signal would be obtained from more than one zone (e.g., Müller et al., 2003b; Rusk et al., 2011; Breiter et al., 2012; Cruz-Uribe et al., 2017).

Electron probe microanalysis (EPMA) has the advantages of non-destructive testing and high spatial resolution; however, the achievement of high accuracy and precision can be an issue. In trace elemental analysis by EPMA, the precision is typically enhanced by changing the acceleration voltage, increasing the counting time, or increasing the beam current (e.g., Jercinovic et al., 2012; Batanova et al., 2015). In addition, the simultaneous use of multiple crystals for single elements can improve the analytical precision (e.g., Donovan et al., 2011; Goemann et al., 2014).

Some research on improving the accuracy of trace elements in quartz has been performed (e.g., Müller et al., 2003b; Donovan et al., 2011, 2016; Kronz et al., 2012), from which the main factors affecting the analytical accuracy can be summarized as follows:

*Author for correspondence: Shui-Yuan Yang, E-mail: shuiyuanyang@cug.edu.cn

Cite this article: Cui J-Q, Yang S-Y, Jiang S-Y, Xie J (2019) Improved Accuracy for Trace Element Analysis of Al and Ti in Quartz by Electron Probe Microanalysis. *Microsc Microanal* **25**, 47–57. doi:10.1017/S1431927618015672

(a) Quartz lattices are easily damaged at high beam currents, resulting in the migration of elements (e.g., Müller et al., 2003b; van den Kerkhof et al., 2004; Kronz et al., 2012), which changes the characteristic X-ray count intensity over time and leads to inaccurate analytical results. While some research into time-dependent intensity (TDI) behavior at high currents has been carried out, these studies have tended to be on other materials, such as olivine (800 nA, Batanova et al., 2015) and monazite (200 nA, Jercinovic et al., 2008), and it is not clear whether these studies are applicable to quartz. In addition, TDI research on the background is unexplored. The background measurement will be inaccurate if the background intensity exhibits time-dependent variations at high beam currents.

(b) Accurate modeling and measurement of background intensity. The measurement of the background is vitally important for trace element analysis. In EPMA, the two-point background interpolation method is often used. However, the background shape of some elements is not a straight line, but a curved line. The two-point background interpolation method is often not an issue in major element analysis with high peak/background ratios, but it will significantly affect the accuracy of trace elements when the background shape is a curved line or other major element peaks are near the trace element peak. To address this problem, Jercinovic & Williams (2005) used detailed wavelength scanning and overlap peak separation with an advanced multipoint background model to obtain accurate U, Th, and Pb concentrations for monazite dating. Donovan et al. (2011) used the two-point background with exponential curve fitting and blank correction to determine the background intensity of Al in quartz. The exponential fit equation is complex and is currently only available in Probe for EPMA software, or is obtained by manual calculation. Recently, the mean atomic number background calibration curve method in Probe for EPMA software has been applied to correct the background intensity, which can avoid background measurement artifacts (Donovan et al., 2016). The use of blank corrections is often not possible due to the lack of suitable blank samples in most laboratories. Therefore, it is of great significance to determine a simple method to accurately determine the background.

(c) Background interference peaks (such as the interference of Al-Kβ, which may cause background measurement errors) and secondary fluorescence (such as a neighboring feldspar or rutile close to quartz producing an apparent signal of Al-Kα and Ti-Kα within the quartz). While choosing background positions, any possible background interference peaks should be avoided. For secondary fluorescence, it is necessary to maintain a safe distance from the interference mineral or to correct the interference (e.g., Jercinovic & Williams, 2005; Fournelle, 2007; Jercinovic et al., 2012; Kronz et al., 2012). Monte Carlo simulation (e.g., PENEPMA or DTSA-II) can provide guidelines for the spatial extent of possible secondary fluorescence from fluorescing phases.

In this study, we investigate the TDI variations of the peaks of Al and Ti and surrounding background positions at high currents; our aim is to find an analytical method that can improve the accuracy and precision of these measurements. Based on detailed wavelength scanning, the concentration of trace elements in quartz is determined by the multipoint background method, through manual calculation.

Experimental Materials and Establishment of Measurement Protocol

Three samples are used in this experiment: (a) a natural and colorless quartz sample, named Q-Nature; (b) synthetic SiO_2 glass, named Q-Glass; and (c) a reference quartz standard sample with homogeneous Al (154 ± 15 ppm) and Ti (57 ± 4 ppm), named Q-Std, which is from a miarolitic cavity within granite from the Shandong Province, China (Audétat et al., 2015). These samples are embedded in epoxy resin and then polished such that most of the quartz grains are exposed to the surface. The precautions suggested by Zhang & Yang (2016) were used to minimize the difference in carbon film thickness between samples and obtain a uniform coating of approximately 20 nm. The experiment was conducted on a JEOL JXA-8100 with four wavelength-dispersive spectrometers at the State Key Laboratory of Geological Processes and Mineral Resources, China University of Geosciences (Wuhan).

Accelerating Voltage, Beam Current, and Detection Limit

To determine the relationship between the accelerating voltage and the detection limit, measurements of Al (Kα, PETJ) and Ti (Kα, TAP) were determined at different accelerating voltages (15, 20, and 25 kV) and beam currents (100, 200, 300, 400, 500, and 600 nA). The optimal experimental conditions for analysis of Ti and Al in quartz are discussed below.

EPMA for TDI Variations of Elemental X-ray and Backgrounds

The counting stability of Al and Ti in Q-Std was examined with beam diameters of 0 (focused), 1, 2, 5, 10, 15, and 20 μm, at an accelerating voltage of 20 kV and beam current of 500 nA. The "chart record" function in the original equipment manufacturer's probe software was used to record the TDI variations of elemental X-rays upon irradiation with different beam diameters. Under all conditions, the total data acquisition time was 600 s in consecutive 9 s counting intervals (no beam blanking). The X-ray intensities of Al (Kα, TAP) and Ti (Kα, PETJ) were investigated.

In addition, we conducted a TDI study on surrounding background positions of the Al-Kα and Ti-Kα peak, using Q-Std at an accelerating voltage of 20 kV and beam current of 500 nA, to examine the intensity variation of the background.

Detailed Wavelength Scanning

Detailed wavelength scanning of Q-Nature was carried out on the Al region of TAP and the Ti region of PETJ. The scan was run at 10 μm/step (spectrometer units) and 5 s/step with a 20 μm beam diameter, 20 kV accelerating voltage, and 500 nA beam current. This was performed to determine the shape of the background slope, and consequently, suitable locations for obtaining background measurements. In addition, the wavescans allowed us to search for potential interference peaks.

Results and Discussion

Choice of Accelerating Voltage and Beam Current

The results indicate that, with an increase in the accelerating voltage, the detection limit of Al first decreases slightly and then

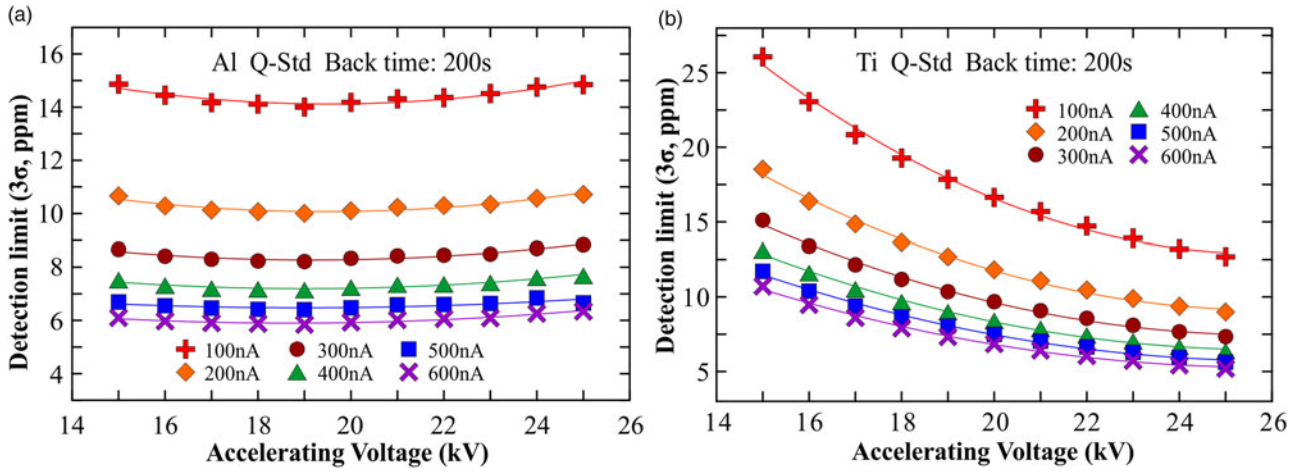

Fig. 1. Detection limit of (**a**) Al and (**b**) Ti in Q-Std as a function of beam current and accelerating voltage.

increases slightly (Fig. 1a). As the accelerating voltage increases, the detection limit of Ti decreases (Fig. 1b). This indicates that, with the increase of X-ray excitation depth, the emission at greater depths of Ti-Kα is not affected by absorption as much as that of Al-Kα (Reed, 2000). To effectively improve the analytical precision and lower the detection limit of Al and Ti in quartz, it is ideal to choose a higher accelerating voltage (we chose an accelerating voltage of 20 kV in this study). However, when the beam current continues to increase to over 500 nA, the effect of raising the beam current to improve the detection limit becomes less noticeable (Fig. 1). Therefore, for the analysis of Al and Ti in quartz, a 20 kV accelerating voltage and a 500-nA beam current were selected.

Processing of Interference

For the analysis of major elements, small interferences have minimal impact, but for trace element analysis, this will cause errors. Therefore, any interference must be determined and accounted for. Four key aspects relating to interference were considered:

(1) Interference peaks: the Al-K$\beta_{1,3}$ peaks (at 86–87 mm on the spectrometer) and an Al-SKβ peak (at ~88 mm on the spectrometer) were found in the background by a detailed wavelength scan (Al region of TAP, Fig. 2a); therefore, it is necessary to avoid these potential background interference peak positions when choosing background positions.

(2) Secondary fluorescence: some neighboring phases that contain Al and Ti (such as rutile, ilmenite, and feldspar) will produce an apparent Ti/Al-signal in the detector which can be mistaken as coming from the quartz. This effect can be modeled using simulation software, such as PENEPMA (Llovet & Salvat, 2017); this program is included in Probe Software's free CalcZAF/Standard software (http://probesoftware.com/download/CalcZAF.msi). In this study, the simulation of secondary fluorescence effects in two mineral pairs (quartz-rutile and quartz-sanidine) were run. Secondary fluorescence can extend to hundreds of micrometers, depending upon the low level present in the real sample; the Monte Carlo modeling can generate apparent values out hundreds of micrometers. Here, we are defining a level of ~10 ppm (K ratio of 0.001%). The modeling results for Al and Ti are given in Fig. 3. For Al excited in an adjacent sanidine, the influence of Al-Kα secondary fluorescence ends at a distance of approximately 16 μm. For Ti-Kα in quartz-rutile, an elevated signal was seen up to a distance of 360 μm. Consequently, for secondary fluorescence, it is necessary to maintain a safe distance from the interference mineral or correct for the interference, if possible (e.g., Jercinovic & Williams, 2005; Fournelle, 2007; Jercinovic et al., 2012; Kronz et al., 2012; Borisova et al., 2018).

(3) "Step": an instrument artifact on PETJ spectrometers is at a position of 82–83 mm (Fig. 2b). The "step" on the wavelength scanning curve can be handled by keeping a safe distance from the "step" when choosing background positions.

(4) "Hole": caused by secondary Bragg diffraction at other lattice planes at some angle to the preferred lattice plane; a "hole" in the background can occur both adjacent to and directly underneath the Ti-Kα X-ray peak position in quartz (Donovan et al., 2011). However, these are not always observed. In our experiment, a "hole" was not seen.

Effect of Beam Current, Beam Diameter, and TDI Variation

At high beam currents, it is very easy for the crystal structure of quartz to be destroyed (e.g., Müller et al., 2003b; van den Kerkhof et al., 2004; Kronz et al., 2012). However, previous studies suggest that a breakdown in the lattice does not appear to affect strongly bonded trace elements (Ti and Fe) (e.g., Kronz et al., 2012). In general, increasing the beam diameter can reduce the TDI variation effectively, but a beam diameter that is too large will cause a loss in spatial resolution. In addition, too large a beam diameter can lead to X-ray defocusing (off the Rowland Circle) on some parts of its outer perimeter. Thus, it would be beneficial to find the smallest possible beam diameter that can still maintain a stable signal intensity.

The signal intensity of Ti in quartz is not as stable as previously reported (e.g., Kronz et al., 2012). At beam diameters of 0, 1, and 2 μm, the signal intensity of Ti-Kα first decreases and then increases gradually. Throughout the process, the signal intensity acquired at a beam diameter of 0, 1, and 2 μm is lower than that at a beam diameter of 20 μm (Fig. 4). At beam diameters of 5, 10, and 20 μm, the Ti signal intensity increases from 5 to 20 μm along a quadratic polynomial curve (Fig. 4). Although

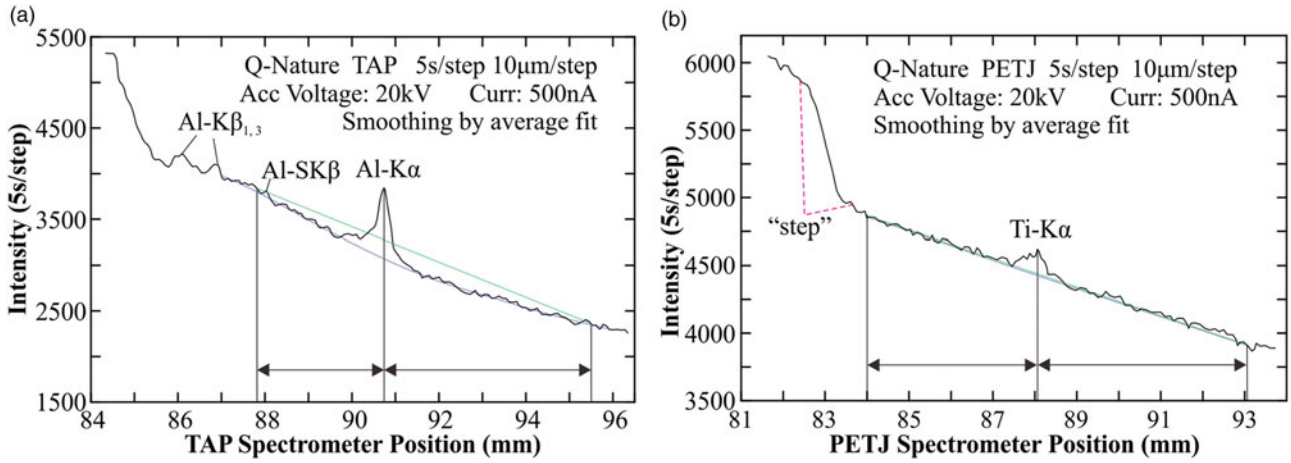

Fig. 2. Wavelength scanning of the (**a**) Al-Kα region of TAP and (**b**) Ti-Kα region of PETJ. The green and blue lines represent the linear (two point) and polynomial interpolations, respectively, of the background.

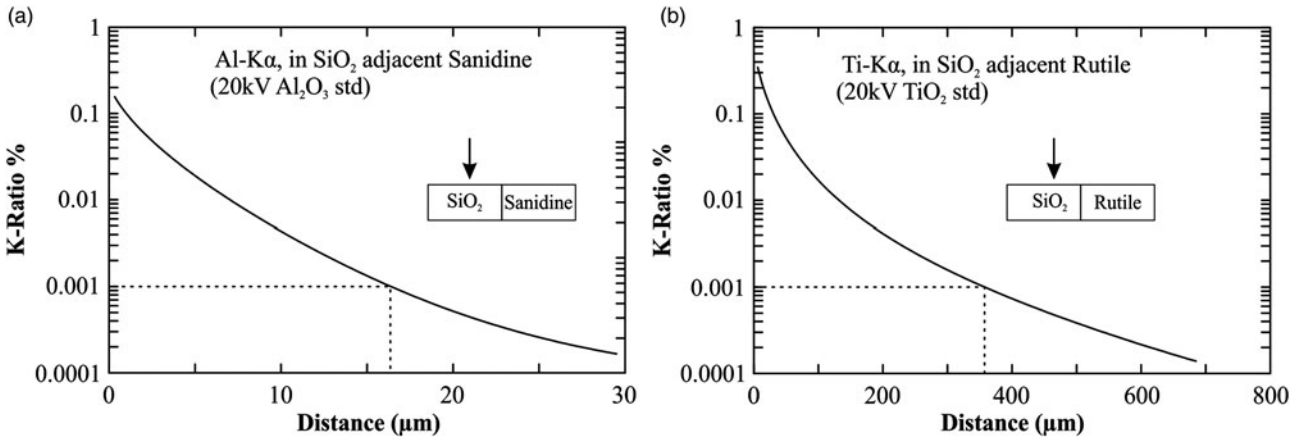

Fig. 3. *k*-ratio profiles for a quartz sample in contact with (**a**) sanidine and (**b**) rutile.

the difference is small, it can have a significant impact on the accuracy of the results. At a beam diameter of 20 μm, the signal intensity of Ti is steady and the best fit line for the data is straight. These results indicate that Ti in quartz also exhibits TDI variation under a small beam diameter and that the characteristic X-ray intensity of Ti decreases rapidly under electron beam bombardment and then varies according to the energy density of the beam.

At beam diameters of 0, 1, and 2 μm, the signal intensity of Al-Kα remains stable initially and then rises rapidly before stabilizing (Fig. 5a). During the analysis, Al had a higher count rate at diameters of 0, 1, and 2 μm relative to 20 μm, especially during the first 100 s. At a beam diameter of 5 μm, the signal intensity of Al-Kα is higher relative to that at 20 μm and rises gradually. At a beam diameter of 10 μm, the signal intensity of Al-Kα first rises and then stabilizes; it remains stable at 15 and 20 μm (Fig. 5a).

The absorbed currents were also monitored during TDI measurements. The absorbed currents are stable at a beam diameter of 20 μm, but decline at 0, 1, 2, 5, 10, and 15 μm; furthermore, the rate of decline decreases from 0 to 15 μm (Fig. 5b). There is a slight increase in the final 200 s of the analyses with beam diameters of 0 and 1 μm (Fig. 5b). This may be related to the destruction of the carbon film under high beam current conditions causing a decrease in conductivity.

The above results show that to ensure the stability of detection, a beam with a diameter of 20 μm is a suitable option at a beam current of 500 nA, but there is a clear loss in spatial resolution. If a small beam diameter is chosen, a lower current must also be chosen; this will reduce the precision of the detection. In these cases, using large spectral crystals or many crystals simultaneously can also improve the precision; however, this is not discussed in this paper.

At high beam currents, the background count of Al-Kα at a beam diameter of 20 μm is lower than that at 5 μm (Figs. 6a, 6b). This indicates that there are some variations in intensity in the background as well. The background count for Ti-Kα is always stable (Figs. 6c, 6d); however, it can be observed, from the quadratic polynomial trend line, that the signal intensity for a beam spot diameter of 5 μm is generally lower than that for one with a diameter of 20 μm (Figs. 6c, 6d). Thus, the background positions on both sides of the Al-Kα and Ti-Kα peak exhibit variations in intensity, and it is necessary to choose a large beam diameter in the analysis process to avoid variations in TDI.

Multipoint Background Method

The results of wavelength scanning (Figs. 2 and 7) indicate that using the traditional two-point background method to detect

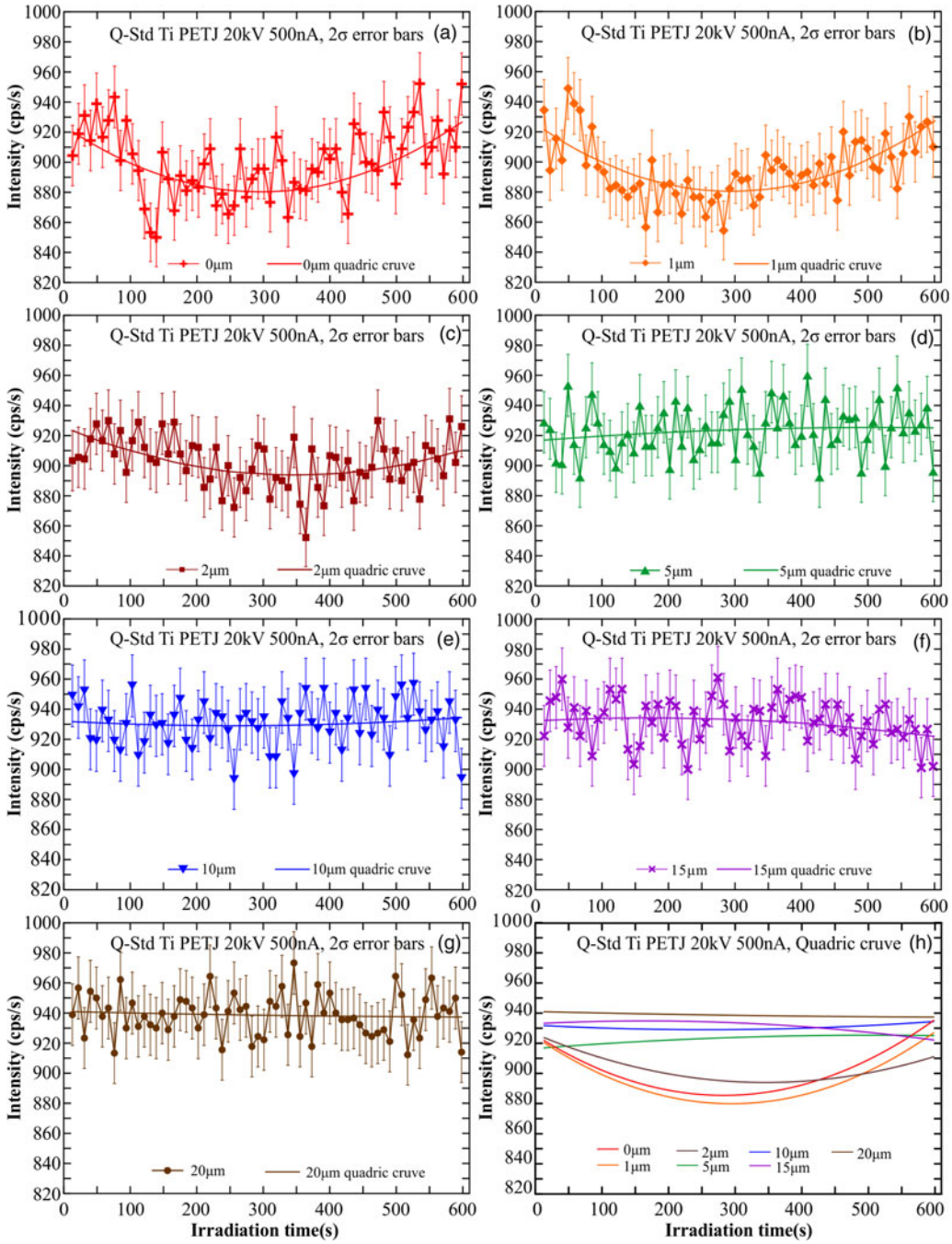

Fig. 4. Ti-Kα counts as functions of beam diameter and time.

elements with a curved background is problematic because it increases the background value. In this study, we used a multipoint background method to determine the background value accurately and obtain accurate quantitative analytical results.

Several points on both sides of the Al-Kα and Ti-Kα peaks were chosen to determine the background value. The background and peak counts were determined using a beam diameter of 20 μm, an accelerating voltage of 20 kV, and a beam current of 500 nA. The counts detected were converted to counts per second and then fitted into a curve equation. In this experiment, quadratic polynomial, exponential, logarithmic, and power functions were used to fit the background curve of Al and Ti in Q-Pure. The resulting curves were compared to those obtained using the traditional two-point background method. After the equation of the fitted curve was obtained, the spectrometer position of the peak was regarded as a variable and brought into the equation, after which the background count at the spectrometer position of the peak can be calculated from the equation of the fitted curve. The net on peak count is obtained by subtracting the background count from the uncorrected on peak count. The element concentration can be obtained by comparing the net count of characteristic X-rays from the sample with the net count from the standard; counts from the sample and standard must be corrected for

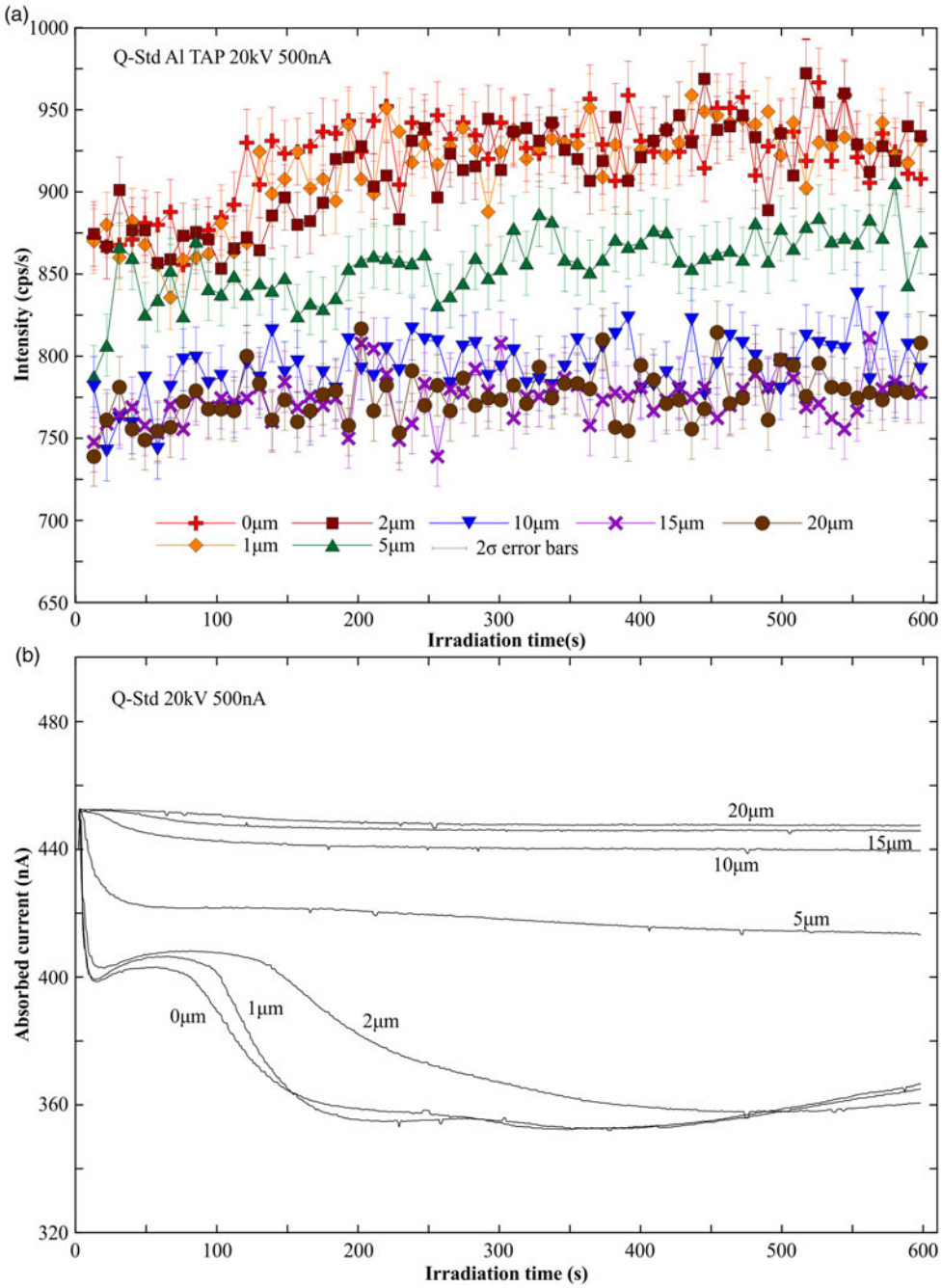

Fig. 5. a: Al-Kα counts as a function of beam diameter and time and (**b**) variations of absorbed current during TDI measurements.

matrix effects. This study used the ZAF (atomic number, absorption, fluorescence) correction.

Comparisons of the fitting results for Al show that the background values obtained by the quadratic, exponential, logarithmic, and power curves are lower than those using the two-point background method, and that the background value obtained by the logarithmic curve is slightly higher than the other three (Fig. 7a). The Al concentration obtained using the different fitting methods is within the range of the reference values, except for the values calculated by the two-point background method, which are lower (Table 1). Comprehensive analysis shows that the results obtained using quadratic, exponential, and power fitting are more reliable. For the Ti background curve, there is no distinction between the background values obtained by the different fitting methods (Fig. 7b). When combined with the data in Table 1, the results obtained by the different fitting curves and two-point background method are very close to the reference values. Thus, all kinds of fitting methods are reasonable to measure Ti.

In this experiment, three samples of Q-Nature, Q-Glass, and Q-Std were used to determine the background count; these were then calculated using the quadratic curve. It was found that the background values from the different samples are very similar (Fig. 8). Ten points were measured on Q-Std with an on peak

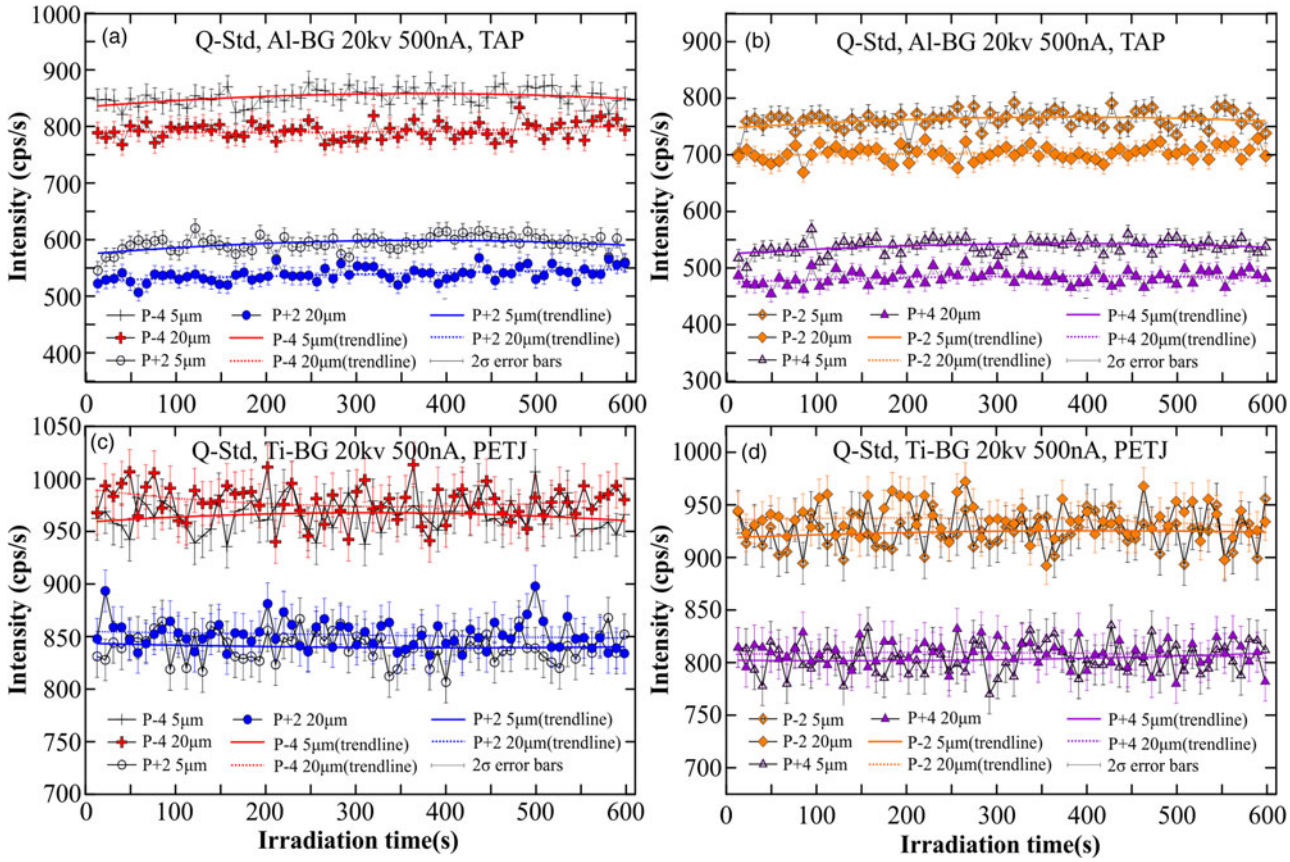

Fig. 6. Background counts of both sides of (**a, b**) Al-Kα and (**c, d**) Ti-Kα peaks as functions of beam diameter and time. "P – N" indicates that the left background position is at a distance of *N* mm from the peak; "P + N" indicates that the right background position is at a distance of *N* mm from the peak (*N* = 2 or 4).

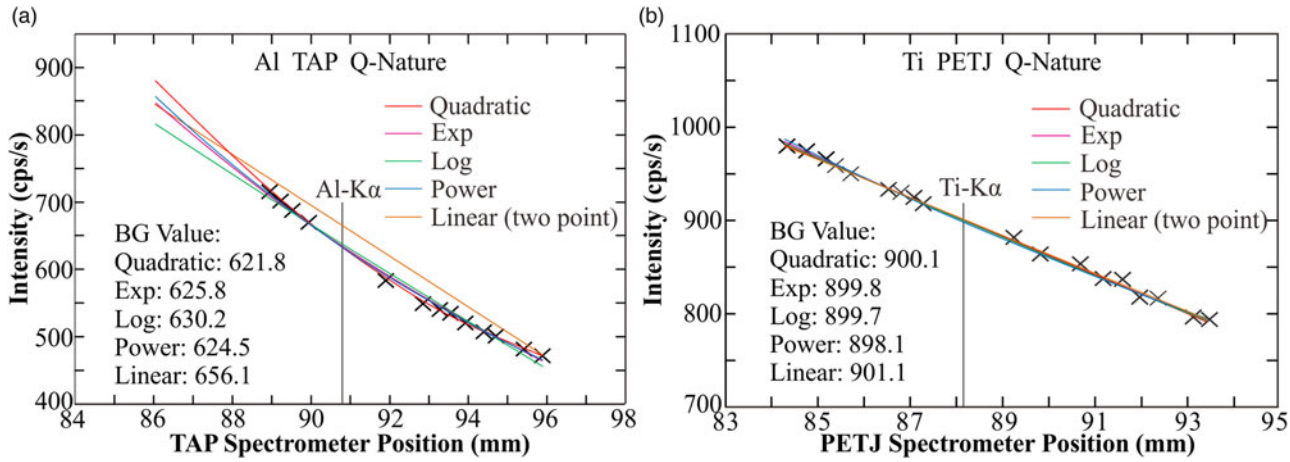

Fig. 7. Fitting background curves of (**a**) Al and (**b**) Ti using different functions.

count time of 200 s. To test whether there was any difference in the backgrounds between the three samples, the Al and Ti content in Q-Std were calculated using the background values from those samples (Table 2). The results reveal that by using the background values from Q-Nature, Q-Std has 158.0 ± 3.4 ppm Al and 55.3 ± 2.0 ppm Ti. If the background values of Q-glass were used, the results were: Al = 158.3 ± 4.3 ppm and Ti = 55.6 ± 2.0 ppm. And if the background values of Q-Std itself were used, the results were: Al = 158.1 ± 5.7 ppm and Ti = 53.9 ± 1.9 ppm. These are all very similar to the reference values (154 ± 15 ppm for Al and 57 ± 4 ppm for Ti; Audétat et al., 2015). Therefore, the background signal from different quartz samples can be applied to other unknown quartz samples being examined, and only the counts of the peaks are measured on the unknown quartz samples to improve efficiency. However, we suggest that a secondary standard (such as the sample Q-Std from Audétat et al., 2015) should

Table 1. Calculation Results of Different Fitting Functions and the Two-Point Background Method.

	Quadratic		Exp		Log		Power		Linear	
Number	Al (ppm)	Ti (ppm)	Al (ppm)	Ti (ppm)	Al (ppm)	Ti (ppm)	Al (ppm)	Ti (ppm)	Al (ppm)	Ti (ppm)
1	155.0	54.4	151.4	54.8	147.3	55.0	152.1	57.1	123.6	53.0
2	156.3	53.8	152.6	54.2	148.6	54.3	153.4	56.4	124.9	52.4
3	163.6	54.3	159.9	54.7	155.8	54.8	160.7	56.9	132.1	52.9
4	154.1	55.6	150.4	56.0	146.3	56.1	151.2	58.2	122.6	54.2
5	154.4	55.9	150.8	56.3	146.7	56.4	151.5	58.5	123.0	54.5
6	160.4	53.1	156.8	53.5	152.7	53.7	157.5	55.8	129.0	51.7
7	159.8	54.1	156.1	54.5	152.1	54.7	156.9	56.8	128.4	52.7
8	157.1	54.5	153.5	54.9	149.4	55.1	154.2	57.2	125.7	53.1
9	161.7	58.5	158.1	58.9	154.0	59.0	158.9	61.1	130.3	57.1
10	161.4	59.0	157.8	59.4	153.7	59.5	158.5	61.6	130.0	57.6
Avg	158.4	55.3	154.7	55.7	150.7	55.9	155.5	58.0	127.0	53.9
Stdev	3.4	2.0	3.4	2.0	3.4	2.0	3.4	2.0	3.4	2.0

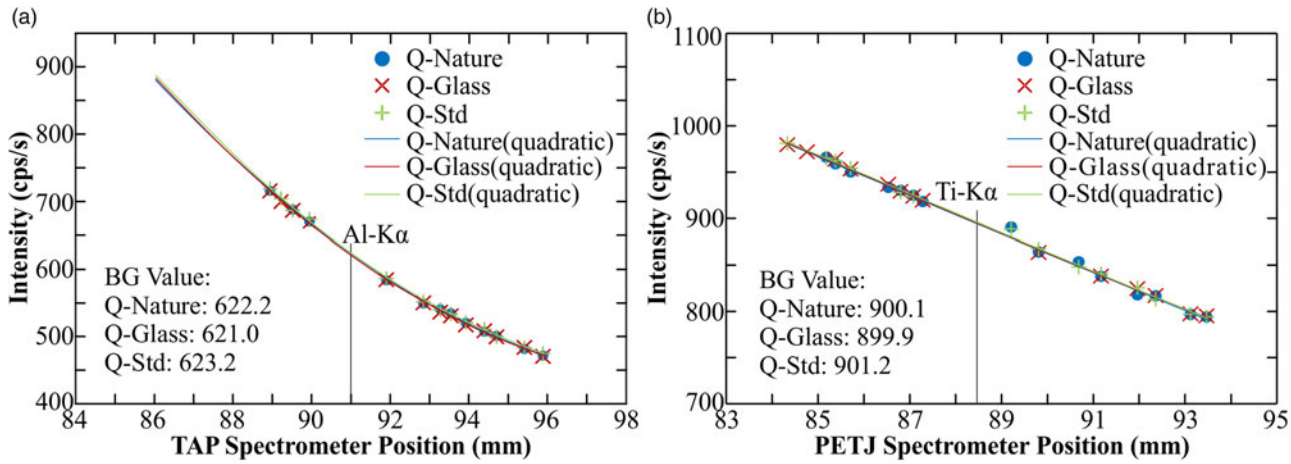

Fig. 8. Quadratic polynomial fitting background curve based on Q-Nature, Q-Glass, and Q-Std samples of (**a**) Al and (**b**) Ti.

Table 2. Simultaneous Detection of Al and Ti in Q-Std Using Three Samples as Background Values.

	Q-Pure		Q-Glass		Q-Std	
Number	Al (ppm)	Ti (ppm)	Al (ppm)	Ti (ppm)	Al (ppm)	Ti (ppm)
1	154.7	53.1	156.5	53.4	163.6	51.7
2	155.9	59.0	157.8	59.2	155.0	57.5
3	163.2	53.8	155.6	54.0	162.3	52.4
4	153.7	58.5	149.1	58.7	152.8	57.0
5	154.1	54.1	155.9	54.4	153.2	52.7
6	160.1	55.9	161.9	56.1	159.2	54.4
7	159.4	54.3	161.3	54.5	158.5	52.9
8	156.8	55.6	158.6	55.8	155.8	54.1
9	161.4	54.4	163.3	54.7	160.5	53.0
10	161.1	54.5	162.9	54.8	160.1	53.1
Avg	158.0	55.3	158.3	55.6	158.1	53.9
Stdev	3.4	2.0	4.3	2.0	3.7	1.9

Table 3. Analytical Results of Al in a Secondary Q-Std Standard Sample (Al = 154 ± 15 ppm) Using Different Currents and Beam Diameters.

Number	20 kV 500 nA 5 μm	20 kV 500 nA 10 μm	20 kV 500 nA 20 μm	20 kV 300 nA 5 μm	20 kV 300 nA 10 μm	20 kV 300 nA 20 μm	20 kV 100 nA 5 μm	20 kV 100 nA 10 μm	20 kV 100 nA 20 μm
1	226.9	176.6	159.5	223.3	163.9	163.8	230.5	162.2	156.3
2	232.6	181.0	154.4	234.8	162.4	150.2	206.2	159.0	154.4
3	229.8	171.9	155.8	242.2	167.6	156.7	215.4	161.3	150.8
4	227.5	173.7	157.7	243.5	169.0	152.9	218.1	159.5	154.4
5	233.2	174.7	157.8	220.0	159.5	153.7	214.0	166.8	148.0
6	224.9	172.5	158.2	218.7	167.9	154.0	207.6	164.1	155.8
7	257.0	179.3	150.6	214.3	163.5	151.7	282.3	159.0	155.4
8	230.1	172.7	153.3	215.4	161.5	152.2	212.2	163.6	159.0
9	244.2	177.9	156.9	254.5	157.8	152.3	198.9	157.7	156.3
10	221.0	173.6	160.8	243.5	160.3	156.0	219.5	166.8	156.7
Avg	232.7	175.4	156.5	229.8	163.3	154.3	220.5	162.0	154.7
Stdev	10.5	3.1	3.0	14.4	3.8	3.8	23.3	3.3	3.2

Table 4. Analytical Results of Ti in a Secondary Q-Std Standard Sample (Ti = 57 ± 4 ppm) Using Different Currents and Beam Diameters.

Number	20 kV 500 nA 5 μm	20 kV 500 nA 10 μm	20 kV 500 nA 20 μm	20 kV 300 nA 5 μm	20 kV 300 nA 10 μm	20 kV 300 nA 20 μm	20 kV 100 nA 5 μm	20 kV 100 nA 10 μm	20 kV 100 nA 20 μm
1	37.9	50.0	54.5	35.0	42.7	52.6	44.4	55.0	66.8
2	35.9	51.6	58.8	20.3	42.7	58.1	51.0	49.1	51.0
3	35.5	53.4	62.6	32.8	47.1	56.1	33.9	53.7	58.9
4	32.3	53.4	57.2	27.1	52.1	63.5	29.9	59.6	64.2
5	39.0	49.7	51.4	27.5	47.1	58.3	43.1	62.9	64.9
6	28.2	52.3	56.8	34.3	52.6	56.7	37.2	72.1	62.2
7	13.6	46.7	55.0	27.1	45.1	51.5	49.7	62.2	51.0
8	28.8	49.4	53.3	23.1	45.1	53.4	38.5	58.9	58.3
9	35.1	50.4	55.5	28.4	44.2	59.2	49.1	54.3	55.6
10	33.0	47.1	56.3	37.6	51.2	55.6	35.9	60.9	51.7
Avg	31.9	50.4	56.1	29.3	47.0	56.5	41.3	58.9	58.5
Stdev	7.3	2.3	3.1	5.5	3.8	3.5	7.3	6.4	6.0

be selected as a monitor sample to evaluate data quality and determine whether the calculated background curve is still applicable. Furthermore, a more uniform quartz sample can be used in the background test and a large beam diameter and high beam current can also be used to determine the background value accurately.

Further Verifications of the Effect of Variations in TDI

After the Q-Nature sample was used to determine the background with a beam diameter of 20 μm, the content of Al and Ti in the secondary Q-Std standard sample was determined at beam currents of 100, 300, and 500 nA (Tables 3 and 4) with beam diameters of 5, 10, and 20 μm, respectively. According to the results, analysis of Al using a beam diameter of 5 μm shows a range of values that are clearly higher than the reference value and are affected significantly by variations in the TDI. With a beam spot diameter of 5 μm for Ti, the results are clearly lower than the reference value range (Table 4), which is significantly affected by the variation in TDI. This is different from the findings of Kronz et al. (2012). Therefore, a small current must be used with small beam spot diameters and the precision should be improved using other methods.

In addition, the count rates of backgrounds in the Q-Std sample were determined at an accelerating voltage of 20 kV and a

Table 5. Analytical Results of Al and Ti in a Secondary Q-Std Standard Sample Using Beam Diameters of 5, 10, and 20 μm to Measure Background values.

	Al (ppm)			Ti (ppm)		
Number	5 μm	10 μm	20 μm	5 μm	10 μm	20 μm
1	74.1	142.3	164.3	77.5	64.0	60.2
2	67.3	135.5	157.5	74.1	60.5	56.8
3	69.8	138.0	160.0	71.5	58.0	54.2
4	72.1	140.4	162.4	78.0	64.5	60.7
5	72.1	140.4	162.4	75.8	62.3	58.5
6	72.6	140.9	162.9	74.0	60.5	56.7
7	69.9	138.1	160.1	75.3	61.8	58.1
8	68.8	137.1	159.0	81.2	67.7	63.9
9	66.4	134.7	156.7	76.5	63.0	59.2
10	71.9	140.1	162.1	82.3	68.7	65.0
Avg	70.5	138.7	160.7	76.6	63.1	59.3
Stdev	2.5	2.5	2.5	3.3	3.3	3.3

beam current of 500 nA, with beam diameters of 5, 10, and 20 μm, respectively. The count rates of peaks of Al and Ti in the secondary Q-Std standard sample were then determined at beam currents of 500 nA and a beam diameter of 20 μm. The Al and Ti contents in the secondary Q-Std standard sample using these conditions were obtained (Table 5). Analysis of Al obtained at a background of 5 μm shows a range of values that are clearly lower than the reference value, and similar analyses of Ti show a range of values that are clearly higher than the reference value. When the backgrounds were determined at 20 μm, both the Al and Ti results were close to the reference value. These results indicate that there are indeed some variations in background intensity when different beam diameters are used.

Conclusions

At high beam currents, the crystal structure of quartz can be destroyed easily and element migration can occur, affecting the accuracy of trace element analysis using EPMA. This paper presents a detailed TDI study on the peaks of Al-Kα and Ti-Kα and both sides of these peaks at high beam currents (500 nA). The peaks of Al-Kα and Ti-Kα were found to show variations in TDI, and the background on both sides of the peaks were found to have some variations in intensity at high beam currents and small beam diameters. The signal intensity of Al initially increases over a very short period when the beam diameter is small and is stable only for large beam spot diameters. The signal intensity of the Ti in quartz, however, is not stable; this has not been described in previous research (Kronz et al., 2012). The Kα peak signal intensity of Ti using small beam diameters is initially lower than that using large beam diameters over a short time period. Although this difference is small, it can have a great impact on the accuracy of the detection results. Therefore, a large beam diameter is needed to avoid variations in TDI at high beam currents.

Detailed wavelength scanning indicates that the background of Al in quartz is a concave curve, not a straight line. In this case, the traditional two-point background method will produce incorrect results. By using the multipoint background method to fit the background curve equation and calculate the background value, the detection accuracy can be improved greatly. For the Ti in quartz, the background is approximately a straight line, and the results of the two-point background method are no different than those of the multipoint background method. In addition, measurements of the background count rate for three different quartz samples were all identical, suggesting that background Al and Ti values can be measured from any quartz sample and applied to the sample of interest, saving time and reducing sample damage.

Author ORCIDs. Shui-Yuan Yang 0000-0003-3594-8865

Acknowledgments. The authors wish to thank Andreas Audétat for providing the reference quartz standard sample. This work was supported by the National Key R&D Plan of China (Grant No. 2017YFC0601404) and the National Natural Science Foundation of China (No. 41773040). The authors are grateful to three anonymous reviewers for providing valuable comments and suggestions that helped to improve this manuscript significantly. Special thanks to John Fournelle and Donggao Zhao for correcting the grammar and syntax of the manuscript. We also thank Masashi Watanabe for his editorial work.

References

Audétat A (2013). Origin of Ti-rich rims in quartz phenocrysts from the Upper Bandelier Tuff and the Tunnel Spring Tuff, southwestern USA. *Chem Geol* **360–361**, 99–104.

Audétat A, Garbe-Schönberg D, Kronz A, Pettke T, Rusk B, Donovan JJ & Lowers HA (2015). Characterisation of a natural quartz crystal as a reference material for microanalytical determination of Ti, Al, Li, Fe, Mn, Ga and Ge. *Geostand Geoanal Res* **39**, 171–184.

Batanova VG, Sobolev AV & Kuzmin DV (2015). Trace element analysis of olivine: High precision analytical method for JEOL JXA-8230 electron probe microanalyser. *Chem Geol* **419**, 149–157.

Borisova AY, Zagrtdenov NR, Toplis MJ, Donovan JJ, Llovet X, Asimow PD, De Parseval P & Gouy S (2018). Secondary fluorescence effects in microbeam analysis and their impacts on geospeedometry and geothermometry. *Chem Geol* **490**, 22–29.

Breiter K, Svojtka M, Ackerman L & Švecová K (2012). Trace element composition of quartz from the Variscan Altenberg–Teplice caldera (Krušné

hory/Erzgebirge Mts, Czech Republic/Germany): Insights into the volcano-plutonic complex evolution. *Chem Geol* **326–327**, 36–50.

Cruz-Uribe AM, Mertz-Kraus R, Zack T, Feineman MD, Woods G & Jacob DE (2017). A new LA-ICP-MS method for Ti in quartz: Implications and application to high pressure rutile-quartz veins from the Czech Erzgebirge. *Geostand Geoanal Res* **41**, 29–40.

Donovan JJ, Lowers HA & Rusk BG (2011). Improved electron probe microanalysis of trace elements in quartz. *Am Mineral* **96**, 274–282.

Donovan JJ, Singer JW & Armstrong JT (2016). A new EPMA method for fast trace element analysis in simple matrices. *Am Mineral* **101**, 1839–1853.

Drivenes K, Larsen RB, Müller A & Sørensen BE (2016). Crystallization and uplift path of late Variscan granites evidenced by quartz chemistry and fluid inclusions: Example from the Land's End granite, SW England. *Lithos* **252–253**, 57–75.

Fournelle J (2007). The problem of secondary fluorescence in EPMA in the application of the Ti-in-zircon geothermometer and the utility of PENEPMA Monte Carlo Program. *Microsc Microanal* **13**(Suppl 2), 1390–1391.

Frelinger SN, Ledvina MD, Kyle JR & Zhao D (2015). Scanning electron microscopy cathodoluminescence of quartz: Principles, techniques and applications in ore geology. *Ore Geol Rev* **65**, 840–852.

Garate-Olave I, Müller A, Roda-Robles E, Gil-Crespo PP & Pesquera A (2017). Extreme fractionation in a granite–pegmatite system documented by quartz chemistry: The case study of Tres Arroyos (Central Iberian Zone, Spain). *Lithos* **286**, 162–174.

Goemann K, Vasyukova OV, Kamenetsky VS, Rae CMM & Wilson NC (2014). Determination of trace elements in quartz by combined EPMA and CL microspectrometry. *Microsc Microanal* **20**, 718–719.

Jercinovic MJ & Williams ML (2005). Analytical perils (and progress) in electron microprobe trace element analysis applied to geochronology: Background acquisition, interferences, and beam irradiation effects. *Am Mineral* **90**, 526–546.

Jercinovic MJ, Williams ML, Allaz J & Donovan JJ (2012). Trace analysis in EPMA. *IOP Conference Series-Materials Science and Engineering* 32, p. 1–22.

Jercinovic MJ, Williams ML & Lane ED (2008). In-situ trace element analysis of monazite and other fine-grained accessory minerals by EPMA. *Chem Geol* **254**, 197–215.

Kronz A, Van Den KERKHOF AM & Müller A, 2012. Analysis of low element concentrations in quartz by electron microprobe. In *Quartz: Deposits, Mineralogy and Analytics*, Götze J. & Möckel R. (Eds.), pp. 191–217. Berlin, Heidelberg: Springer.

Larsen RB, Henderson I, Ihlen PM & Jacamon F (2004). Distribution and petrogenetic behaviour of trace elements in granitic pegmatite quartz from South Norway. *Contrib Mineral Petrol* **147**, 615–628.

Larsen RB, Jacamon F & Kronz A (2009). Trace element chemistry and textures of quartz during the magmatic hydrothermal transition of Oslo Rift granites. *Mineral Mag* **73**, 691–707.

Llovet X & Salvat F (2017). PENEPMA: A Monte Carlo program for the simulation of X-ray emission in electron probe microanalysis. *Microsc Microanal* **23**, 634–646.

Müller A, Herrington R, Armstrong R, Seltmann R, Kirwin DJ, Stenina NG & Kronz A (2010). Trace elements and cathodoluminescence of quartz in stockwork veins of Mongolian porphyry-style deposits. *Miner Deposita* **45**, 707–727.

Müller A, Ihlen PM, Snook B, Larsen RB, Flem B, Bingen B & Williamson BJ (2015). The chemistry of quartz in granitic pegmatites of southern Norway: Petrogenetic and economic implications. *Econ Geol* **110**, 1737–1757.

Müller A, René M, Behr HJ & Kronz A (2003a). Trace elements and cathodoluminescence of igneous quartz in topaz granites from the Hub Stock (Slavkovský Les Mts., Czech Republic). *Miner Petrol* **79**, 167–191.

Müller A, Wiedenbeck M, Van Den Kerkhof AM, Kronz A & Simon K (2003b). Trace elements in quartz—a combined electron microprobe, secondary ion mass spectrometry, laser-ablation ICP-MS, and cathodoluminescence study. *Eur J Mineral* **15**, 747–763.

Reed SJB (2000). Quantitative trace analysis by wavelength-dispersive EPMA. *Microchim Acta* **132**, 145–151.

Rusk B, Koenig A & Lowers H (2011). Visualizing trace element distribution in quartz using cathodoluminescence, electron microprobe, and laser ablation-inductively coupled plasma-mass spectrometry. *Am Mineral* **96**, 703–708.

Rusk BG, Lowers HA & Reed MH (2008). Trace elements in hydrothermal quartz: Relationships to cathodoluminescent textures and insights into vein formation. *Geology* **36**, 547–550.

Tanner D, Henley RW, Mavrogenes JA & Holden P (2013). Combining *in situ* isotopic, trace element and textural analyses of quartz from four magmatic-hydrothermal ore deposits. *Contrib Mineral Petr* **166**, 1119–1142.

Van Den Kerkhof AM, Kronz A, Simon K & Scherer T (2004). Fluid-controlled quartz recovery in granulite as revealed by cathodoluminescence and trace element analysis (Bamble sector, Norway). *Contrib Mineral Petr* **146**, 637–652.

Wark DA & Watson EB (2006). Titaniq: A titanium-in-quartz geothermometer. *Contrib Mineral Petr* **152**, 743–754.

Wiebe RA, Wark DA & Hawkins DP (2007). Insights from quartz cathodoluminescence zoning into crystallization of the Vinalhaven granite, coastal Maine. *Contrib Mineral Petr* **154**, 439–453.

Zhang RX & Yang SY (2016). A mathematical model for determining carbon coating thickness and its application in electron probe microanalysis. *Microsc Microanal* **22**, 1374–1380.